Field electron emission enhancement in lithium implanted and annealed nitrogen-incorporated nanocrystalline diamond films

KAMATCHI JOTHIRAMALINGAM, Sankaran; Srinivasu, K.; Yeh, C. J.; Thomas, J. P.; DRIJKONINGEN, Sien; POBEDINSKAS, Paulius; Sundaravel, B.; Leou, K. C.; Leung, K. T.; VAN BAEL, Marlies; Schreck, M.; Lin, I. N. & HAENEN, Ken (2017)
Field electron emission enhancement in lithium implanted and annealed nitrogen-incorporated nanocrystalline diamond films. In: APPLIED PHYSICS LETTERS, 110(26), p. 1-5 (Art N° 261602).

DOI: 10.1063/1.4990393
Handle: http://hdl.handle.net/1942/24317

Field electron emission enhancement in lithium implanted and annealed nitrogen-incorporated nanocrystalline diamond films

K. J. Sankaran,[1,2] K. Srinivasu,[3] C. J. Yeh,[3] J. P. Thomas,[4] S. Drijkoningen,[1,2] P. Pobedinskas,[1,2] B. Sundaravel,[5] K. C. Leou,[3] K. T. Leung,[4] M. K. Van Bael,[1,2] M. Schreck,[6] I. N. Lin[7,a)] and K. Haenen[1,2,a)]

[1]*Institute for Materials Research (IMO), Hasselt University, 3590 Diepenbeek, Belgium.*

[2]*IMOMEC, IMEC vzw, 3590 Diepenbeek, Belgium.*

[3]*Department of Engineering and System Science, National Tsing Hua University, Hsinchu, Taiwan 30013, Republic of China.*

[4]*WATLab and Department of Chemistry, University of Waterloo, Waterloo, Ontario N2L3G1, Canada.*

[5]*Materials Science Group, Indira Gandhi Centre for Atomic Research, Kalpakkam 603102, India.*

[6]*Institute of Physics, University of Augsburg, 86135 Augsburg, Germany.*

[7]*Department of Physics, Tamkang University, Tamsui 251, Taiwan, Republic of China.*

[a)]Electronic mail: inanlin@mail.tku.edu.tw and ken.haenen@uhasselt.be

---

Field electron emission (FEE) properties of nitrogen-incorporated nanocrystalline diamond films were enhanced due to Li-ion implantation/annealing processes. Li-ion implantation mainly induced the formation of electron trap centers inside diamond grains, whereas post-annealing healed the defects and converted the *a-C* phase into nanographite, forming conduction channels for effective transport of electrons. This resulted in high electrical conductivity of 11.0 S/cm and enhanced FEE performance with low turn-on field of 10.6 V/μm, high current density of 25.5 mA/cm^2 (at 23.2 V/μm) and high lifetime stability of 1,090 min for nNCD films.

The superior field electron emission (FEE) properties of nanocrystalline diamond (NCD) film as compared to undoped microcrystalline diamond (MCD) films, create the possibility for this material to be the better material for cold cathode field emitters.[1–3] The sp^2-bonded carbon in the grain boundaries of NCD films is the genuine factor for the enhanced FEE properties of these films as

compared with MCD films.[4,5] Though, the non-diamond carbon is not conductive enough restricting the FEE characteristics achievable for NCD films. Facilitating the formation of nanographitic phases in the grain boundaries due to nitrogen addition (> 20%) in CH_4/Ar plasma can improve the electrical conductivity (EC) that enhances the FEE properties of diamond films. However, high growth temperature (about 700°C) is entailed to activate the dopants for creating the good EC in the diamond films and as the growth mechanism is still not clear the reproducible growth of the films is made very difficult.[6,7]

On the other hand, theoretical studies have predicted that lithium should act as a shallow donor in diamond in interstitial sites.[8] Doping diamond with lithium is achieved *ex-situ* by implantation,[9] diffusion (including electro-diffusion),[10,11] adsorption[12] or *in-situ* via the addition of Li to the gas phase during diamond growth.[13] Possibly, due to their high chemical activity, Li atoms do not occupy single interstitial positions but aggregate or couple with other impurities and defects.[14] Other theoretical calculations envisage a low activation energy for Li diffusion in the crystal lattice of diamond. Nevertheless, attempts to incorporate Li into bulk diamond were unsuccessful.[15] Smith *et al.*[16] reveals that Li-ion implantation into polycrystalline diamond films does exhibit pronounced diffusion of Li to the grain boundary phases of the diamond films after annealing at 1000°C and above. Consequently, Li ions are suitable for ion implantation into NCD films to activate the formation of nanographitic phases in the grain boundaries so as to enhance the FEE properties for these films.

In this context, nitrogen incorporated nanocrystalline diamond (nNCD) films were implanted by Li ions followed by annealing at 1000 °C for obtaining improved EC and FEE characteristics of nNCD films. The effects of Li-ion implantation/annealing processes on the microstructural evolution of nNCD films were investigated in detail using transmission electron microscopy (TEM) and X-ray photoelectron spectroscopy (XPS). The potential mechanism of enhanced EC and FEE properties of nNCD films is the induction of nanographitic phases in the grain boundaries of nNCD films due to Li-ion implantation/annealing processes.

The nNCD films were grown on silicon substrates (1 cm × 1 cm) using an ASTeX 6500 series microwave plasma enhanced chemical vapor deposition system. Prior to nNCD film growth, the silicon substrates were nucleated with a water based state-of-the-art colloidal suspension of 5 nm detonation nanodiamonds.[17] The nNCD film was deposited in a gas mixture of CH_4(6%), H_2(89%) and N_2(5%) with flow rates of 18, 267 and 15 sccm, a microwave power of 2500 W, a pressure of 20 Torr and a substrate temperature of 540^{o}C, respectively. The substrate temperature was measured

using a single color optical pyrometer. It should be noted that 5% N_2 was added to the CH_4/H_2 plasma to decrease the grain size of the diamond films and to increase the proportion of grain boundaries phase in the films, both in thickness and number density.[18] The nNCD deposition was carried out for 2 h to reach a thickness of 500 nm. The characteristics of pristine nNCD films are illustrated in Fig. S1.

Lithium-ion implantations were performed at room temperature with an implantation energy of 50 keV (EATON, 200 kV). TRIM software was used to evaluate the trajectory of the Li ions and to estimate the critical dose for transforming the sp^3 bonds to sp^2 bonds.[19] 50 keV Li has a range of 174 nm with a standard deviation (longitudinal straggling) of 35 nm in diamond, as calculated by TRIM (Fig. S2). The pristine, non-implanted nNCD films are designated as Li0. Several nNCD films were grown using the same growth parameters and were undergone implantations using ion doses of 10^{12}–10^{15} ions/cm^2, which were called Li12, Li13, Li14 and Li15 samples, respectively. Moreover, the Li15 films were further annealed at 1000^{o}C for 30 min under vacuum (10^{-6} Torr) and are designated as Li15A films. The films were still on the Si substrates during post-annealing.

Hall measurements in a van der Pauw configuration (ECOPIA HMS-3000) were carried out to examine the conductive behavior of the Li-ion implanted nNCD films. Curve I (closed symbols) in Fig. 1(a) shows that the EC of Li0 films is low and the EC of Li-ion implanted nNCD films increases monotonously with increasing ion dosage. But the extent of the increase is limited. The EC value reached only around 7.8×10^{-4} S/cm for Li15 films. Interestingly, post-annealing of Li15 films abruptly increased the EC of the films to a large value of 11.0 S/cm with a carrier concentration of 2.4×10^{18} cm^{-3} and mobility values of ~55 cm^2/V s. The obtained EC value of Li15A films is comparable with that of the other ion implanted diamond films[20–22] [see Table SI(a)].

The FEE properties of the samples were measured with an electrometer (Keithley 2410) using a parallel cathode–anode set-up at pressure below 10^{-6} Torr,[7] where the cathode is the diamond films and the anode is a molybdenum rod of diameter 2 mm. The FEE characteristics of the materials were explained using the Fowler-Nordheim (F-N) theory.[23] The turn-on field (E_0) was designated as the lowest value of the F-N plots, corresponding to the intersection of the low and high electric field segments. The Li0 films exhibit a large E_0 value of 25.6 V/μm with a low current density (J) of 4.5 mA/cm^2 at an applied field of 46.4 V/μm [curve I, Fig. 1(b)]. The E_0 value, [curve II (open symbols), Fig. 1(a)], decreased consistently with the dosage of Li-ion implantation. The Li15 films show a smaller E_0 value of 19.6 V/μm and J of 8.4 mA/cm^2 at an applied field of 35.8 V/μm [curve II, Fig. 1(b)]. After post-annealing process, the E_0 value lowered tremendously to 10.6 V/μm for Li15A

films and shows a high J of 25.5 mA/cm^2 at an applied field of 23.2 V/μm [curve III, Fig. 1(b)]. The effective work functions (φ_{eff}) of these diamond films calculated from the slope of the F-N plots [inset of Fig. 1(b)] are $(\varphi_{eff})_{Li0}$ = 0.053 eV for Li0 films, $(\varphi_{eff})_{Li15}$ = 0.047 eV for Li15 films, and $(\varphi_{eff})_{Li15A}$ = 0.021 eV for Li15A, revealing a low φ_{eff} value for nNCD films due to Li-ion implantation/annealing. The improvement in FEE properties due to Li-ion implantation/annealing processed is correlated closely with the increment in EC of the films. The effect of Li-ion implantation in modifying the FEE properties of nNCD films is shown as the variation in *J-E* curves against the dosage of Li-ions in Fig. S3. The data presented in these figures are the average of FEE properties of many nNCD based FEE cathodic devices which were tested in the same configuration.

The J versus time curve is displayed in Fig. 1(c), which signifies that the emission current for Li15A films sustained a period of 1090 min at a J value of 5.05 mA/cm^2, corresponding to a working field of 18.0 V/μm. Conversely, Li15 films show a lifetime stability only up to a period of 650 min at a working field of 34.6 V/μm corresponding to a J of 5.03 mA/cm^2 [inset of Fig. 1(c)]. The Li0 films show even shorter lifetime (360 min at a working field of 44.6 V/μm corresponding to a J of 3.03 mA/cm^2 (Fig. S4). The Li15A films are much more robust (lifetime > 1000 min, even at high current density), compared with other conducting diamond films summarized in Table SI,[20–22,24–27] which is an advantageous feature from a device application point of view.

The results described above indicated that annealing after Li-ion implantation enhanced the EC and FEE properties of nNCD films dramatically. To understand the genuine factor enhancing these properties, the characteristics of the Li15 films were investigated in detail. The scanning electron microscopy (SEM; FEI Quanta 200 FEG microscope) image shown in Fig. 2(a) depicts that the Li15 films have an equi-axed nano-sized granular structure with a very smooth surface. It should be mentioned that the SEM morphology of Li0 films is similar to those of Li15 films, i.e., the surface morphology of the nNCD films changed insignificantly after Li-ion implantation [Fig. S1(a)]. It looks similar even after post-annealing as shown in Fig. 2(b) for the SEM micrograph of the Li15A films. This phenomenon implies that the bombardment damage on the carbon atoms of diamond is very small due to the light weight of Li ions.

The inset of Fig. 2(a) shows the micro-Raman spectra (Horiba Jobin-Yvon T64000 spectrometer, λ = 488.0 nm) of the Li15 and Li15A films, which were fitted using the multi-peak Gaussian function. Spectrum I in this figure shows that the Raman spectrum of the Li15 films contains a sharp peak at 1334 cm^{-1} corresponding to sp^3-bonded carbon ("dia"), and a broadened peak at around 1365 cm^{-1} (D-band) corresponding to disordered carbon. The G-band is observed at

around 1530 cm^{-1}, which is usually observed between 1500 and 1600 cm^{-1}.[28] There also exist peaks at around 1140 cm^{-1} and 1520 cm^{-1}, which are ascribed to the ν_1 and ν_3 modes of *trans*-polyacetylene (*t*-PA) present in the grain boundaries.[28] It should be mentioned that the broadened diamond peak is normally observed for the Li15 films due to the smallness in grain size (approximately nanometer scale) and also owing to the increasing concentration of a variety of growth defects comprising point defects, twins, internal stress and sp^2 admixtures.[29,30] The Li-ion implantation process does not change the bonding structure for nNCD films profoundly such that the Raman spectrum of Li15 films looks similar to Raman spectrum of Li0 films [inset of Fig. S1(a)]. The annealing after Li-ion implantation alters slightly the characteristics of the Raman spectrum of the films. Spectrum II in the inset of Fig. 2(a) shows higher intensities of D and G bands which indicates amorphization and graphitization type of transitions in the nNCD films due to Li-ion implantation/annealing.[31] A shoulder peak observed at around 1538 cm^{-1} (G*-band) is possibly from the nanocrystalline graphite in the films.[32] A reduction in the intensity of the *t*-PA peaks is observed, which is an indication of the dissociation of C-H bonds in *t*-PA located at the grain boundaries of nNCD films and the conversion of the *t*-PA phases into more stable nanographitic phases.[30]

Moreover, the near-surface characteristics of nNCD films were investigated using XPS (a Thermo-VG Scientific ESCALab 250 microprobe). The C1s peak of Li15 films [inset spectrum I, Fig. 2(b)] is observed at 286.0 eV, which is blue-shifted by 1.0 eV with respect to the normal C1s peak of sp^3 diamond (285.0 ± 0.2 eV).[32] The blue-shift of the C1s peak for the Li15 films is due to the removal of H^-, exposing the dangling bonds, which act as trapping centers for electrons. Notably, in the pristine nNCD films, the H^- ions are supposed to be absorbed in atomic defects (vacancies), compensating for dangling bonds.[33] Trapping of charges in the defect states is the possible reason for the increase in surface charging and the C1*s* blue shift after ion implantation.[34,35] Post-annealing markedly altered the XPS characteristics of the Li15 films. The C1s peak reversely shifted toward the normal C1s peak at 285.0 eV for Li15A films [inset spectrum II, Fig. 2(b)], implying that the surface charges were eliminated due to the post-annealing process. Moreover, the C1s peak was fitted with Lorentzian peaks using Shirley's method to estimate the relative intensities of sp^3 and sp^2 components of Li15 and Li15A films. Spectrum I in the inset of Fig. 2(b) indicates that, for Li15 films, sp^2 bonding is dominant with an intensity of 56.2% while the sp^3 peak has an intensity of 43.8%. Spectrum II in the inset of Fig. 2(b) shows that, after the annealing process, the sp^2 peak intensity increased to 61.4%, while sp^3 peak intensity decreased to 38.6% for Li15A films. Consequently, the annealing process increased markedly the content of the sp^2 phases in Li-ion implanted nNCD films.

Notably, the XPS is a surface sensitive measurement. The percentage of sp^2- and sp^3-bonds estimated from XPS represents the content of these bonds on the surface of Li15 and Li15A films that is not the same as those in the bulk of the films.

Figure 3(a) shows the typical bright field TEM (JEOL, 2100F) micrograph for the Li15A films with the inset showing the corresponding selective area electron diffraction (SAED) pattern. The SAED pattern illustrates that, besides the diffraction rings corresponding to the (111), (220), and (311) lattice planes of diamond, a diffused ring of donut-geometry appears in the center of the SAED pattern indicating the existence of some nanographitic phases in the films. The high-resolution TEM microstructure corresponding to region "A" in Fig. 3(a) is shown in Fig. 3(b). The Fourier transformed (FT) diffractogram corresponding to the entire structure image is shown as the inset of Fig. 3(b) as FT_0. The FT_0 image consists of diffraction spots arranged in ring geometry, indicating the presence of randomly oriented diamond grains. A faint diffuse ring with donut-geometry is observable, implying the existence of nanographite in this material. The existence of diamond and nanographitic phases is highlighted by FT images shown as ft_1 and ft_2, which correspond to regions "1" and "2" in Fig. 3(b), respectively. Furthermore, the plasmon-loss electron energy loss spectroscopy (EELS; Gatan Enfina) of Li15A films [spectrum II in Fig. S5(b)] indicates that there is a hump near 27 eV (S_3-band), which corresponds to crystalline sp^2-bonded carbon, i.e. the nanographitic phase.[36–38] From TEM and EELS investigations, it is noticed that Li-ion implantation/annealing processes induce the formation of nanographitic phases, which is in accord with the Raman and XPS investigations. Presumably, the nanographite phase creates conducting paths for transporting electrons that is the key factor resulting in enhanced EC and FEE properties for Li15A films.

Restated, without the post-annealing process, the incident low kinetic-energy Li ions, which are much lighter than the carbon atoms, do not efficiently interact with the *a-C* (or *t*-PA) phases in the grain boundaries of nNCD films. Instead, they interact with the carbon atoms in diamond grains of nNCD films, inducing the formation of electron trap centers that might deleteriously hinder the EC and FEE behavior of nNCD films. Only after post-annealing, the atomic defects induced in diamond grains were effectively healed and electron trap centers were eliminated. The *a-C* (or *t*-PA) phases were converted into nanographitic phases, which created conducting paths for transporting electrons and thus, enhanced the EC and FEE behaviors of Li15A films. Such behavior is totally different from the case where the ultrananocrystalline diamond (UNCD) films were implanted with heavier ions such as Au[24], Cu[25], or Pt[26] [Table SI(b)]. In those cases, the EC and FEE behavior of UNCD films

were markedly enhanced even when the films were as-implanted. Since the diamond grains in UNCD films are extremely small (~5 nm) and the grain boundaries are relatively thick (~0.1 nm), the incident heavy ions mainly interact with the *t*-PA phase in the grain boundaries, converting *t*-PA into nanographite due to the catalytic effect of the incident ions, which are heavy and energetic, and improving the EC and FEE characteristics of the materials.[24–26] Post-annealing process further enhanced these characteristics.[25,26] The other distinctly different feature between the Li-ion implanted NCD films and the heavy ion implanted UNCD films is that the UNCD films contain very wide grain boundaries, which are susceptible to ion bombardment damage, leading to unsatisfactory lifetime stability of the materials.[26] In contrast, nNCD films consist of relatively large diamond grains (50–80 nm) with much thinner grain boundaries. The nanographitic phases induced in these materials due to Li-ion implantation/annealing processes were sandwiched in between diamond grains that can survive the ion bombardment damage. The Li15A films thus illustrated much better robustness than those of heavy ion-implanted UNCD films, although they did not show as good EC and FEE performances. However, the robustness of FEE materials is of more concern in some device applications such as the case when FEE materials are used as cathode in a microplasma device.[39]

In summary, the enhanced EC and FEE properties were achieved for nNCD films due to Li-ion implantation/annealing. Li-ion implantation induced both electron trap centers and *a-C* phases in these films. Post-annealing healed the atomic defects and converted the *a-C* phase into nanographitic phases. These nanographitic phases enriched the EC of the films which is probably the major reason for the enhanced FEE properties. These properties, viz. a low E_0 of 10.6 V/μm and a high J of 25.5 mA/cm^2, along with a long lifetime stability of 1090 min, renders the Li-ion implanted and annealed films a potential candidate for applications in flat panel displays and high brightness electron sources.

Supplementary Material

See supplementary material for SEM morphology, TEM microstructure, Raman spectrum and lifetime stability measurements of pristine nNCD (Li0) films, the trajectory of Li ions in nNCD films simulated by TRIM software and FEE properties of nNCD films implanted with various Li dosage.

The authors like to thank the financial support of the Research Foundation Flanders (FWO) via Research Projects G.0456.12N and G.0905.12N, and the Methusalem "NANO" network. K. J. Sankaran and P. Pobedinskas are Postdoctoral Fellows of the Research Foundation-Flanders (FWO).

[1]A. N. Obraztsov, and A. A. Zakhidov, Diamond Relat. Mater. **13**, 1044 (2004).

[2]W. Zhu, G. P. Kochanski, and S. Jin, Science **282**, 1471 (1998).

[3]K. Okano, S. Koizumi, S. R. P. Silva, and G. A. J. Amaratunga, Nature **381**, 140 (1996).

[4]H. C. Chen, K. J. Sankaran, S. C. Lo, L. J. Lin, N. H. Tai, C. Y. Lee, and I. N. Lin, J. Appl. Phys. **112**, 103711 (2012).

[5]C. S. Wang, H. C. Chen, H. F. Cheng, and I. N. Lin, J. Appl. Phys. **107**, 034304 (2010).

[6]S. Bhattacharyya, O. Auciello, J. Birrell, J. A. Carlisle, L. A. Curtiss, A. N. Goyette, D. M. Gruen, A. R. Krauss, J. Schlueter, A. Sumant, and P. Zapol, Appl. Phys. Lett. **79**, 1441 (2001).

[7]K. J. Sankaran, J. Kurian, H. C. Chen, C. L. Dong, C. Y. Lee, N. H. Tai, and I. N. Lin, J. Phys. D: Appl. Phys. **45**, 365303 (2012).

[8]J. P. Goss, R. J. Eyre, and P. R. Briddon, Phys. Status Solidi B **245**, 1679 (2008).

[9]R. A. Khmelnitsky, V. V. Saraykin, V. A. Dravin, E. V. Zavedeyev, S. V.Makarov, V. S. Bronsky, and A. A. Gippius, Surf. Coat. Tech. **307**, 236 (2016).

[10]J. te Nijenhuis, G. Z. Cao, P. C. H. J. Smits, W. J. P. van Enkevort, L. J. Giling, P. F. A. Alkemade, M. Nesladek, and Z. Remes, Diamond Relat. Mater. **6**, 1726 (1997).

[11]C. Uzan-Saguy, C. Cytermann, B. Fizgeer, V. Richter, R. Brener, and R. Kalish, Phys. Status Solidi A **193**, 508 (2002).

[12]K. M. O'Donnell, T. L. Martin, M. T. Edmonds, A. Tadich, L. Thomsen, J. Ristein, C. I. Pakes, N. A. Fox, and L. Ley, Phys. Status Solidi A **211**, 2209 (2014).

[13]M. Zamir Othman, P. W. May, N. A. Fox, and P. J. Heard, Diamond Relat. Mater. **44**, 1 (2014).

[14]G. Popovici, T. Sung, S. Khasawinah, M. A. Prelas, J. Appl. Phys. **77**, 5625 (1995).

[15]G. Popovici, R. G. Wilson, T. Sung, M. A. Prelas, and S. Khasawinah, J. Appl. Phys. **77 (10)**, 5103 (1995).

[16]S. P. Smith, M. I. Landstrass, and R. G. Wilson, in A. Benninghoven, K. T. F. Janssen, J. Tumpner and H. W. Werner (eds.), Secondary Ion Mass Spectrometry, SIMS VIII, Wiley, New York, 1992, p. 159.

[17]O. A. Williams, O. Douheret, M. Daenen, K. Haenen, E. Osawa, and M. Takahashi, Chem. Phys. Lett. **445**, 255 (2007).

[18]K. J. Sankaran, N. H. Tai, and I. N. Lin, J. Appl. Phys. **117**, 075303 (2015).

[19]C. Uzan-Saguy, C. Cytermann, B. R. Ritcher, V. M. Shaanan, and R. Kalish, Appl. Phys. Lett. **67**, 1194 (1995).

[20]X. J. Hu, J. S. Ye, H. Hu, X. H. Chen, and Y. G. Shen, Appl. Phys. Lett. **99**, 131902 (2011).

[21]X. J. Hu, J. S. Ye, H. J. Liu, Y. G. Shen, X. H. Chen, and H. Hu, J. Appl. Phys. **109**, 053524 (2011).

[22]R. Arenal, P. Bruno, D. J. Miller, M. Bleuel, J. Lal, and D. M. Gruen, Phys. Rev. B **75**, 195431 (2007).

[23]R. H. Fowler and L. Nordheim, Proc. R. Soc. London, Ser. A **119**, 173 (1928).

[24]K. J. Sankaran, H. C. Chen, B. Sundaravel, C. Y. Lee, N. H. Tai, and I. N. Lin, Appl. Phys. Lett. **102**, 061604 (2013).

[25]K. J. Sankaran, K. Panda, B. Sundaravel, N. H. Tai, and I. N. Lin, J. Appl. Phys. **115**, 063701 (2014).

[26]K. J. Sankaran, K. Panda, B. Sundaravel, N. H. Tai, and I. N. Lin, J. Mater. Chem. C **3**, 2632 (2015).

[27]J. P. Thomas, H. C. Chen, N. H. Tai, and I. N. Lin, ACS Appl. Mater. Interfaces **3**, 4007 (2011).

[28]C. Mapelli, C. Castiglioni, G. Zerbi, and K. Mullen, Phys. Rev. B **60**, 12710 (1999).

[29]A. C. Ferrari, and J. Robertson, Phys. Rev. B: Condens. Matter Mater. Phys. **63**, 121405 (2001).

[30]A. Ilie, A. C. Ferrari, T. Yagi, S. E. Rodil, J. Robertson, E. Barborini, and P. Milani, J. Appl. Phys. **90**, 2024 (2001).

[31]R. Kalish, Carbon **37**, 781 (1999).

[32]S. Talapatra, P. G. Ganesan, T. Kim, R. Vajtai, M. Huang, M. Shima, G. Ramanath, D. Srivastava, S. C. Deevi, and P. M. Ajayan, Phys. Rev. Lett. **95**, 097201 (2005).

[33]D. Zhou, T. G. McCauley, L. C. Qin, A. R. Krauss, and D. M. Gruen, J. Appl. Phys. **83**, 540 (1998).

[34]A. Hoffman, I. Andrienko, D. N. Jamieson, and S. Pawar, Appl. Phys. Lett. **86**, 044103 (2005).

[35]Y. Fan, A. G. Fitzgerald, P. John, C. E. Troupe, and J. I. B. Wilson, Surf. Interface Anal. **34**, 703 (2002).

[36]D. M. Gruen, S. Liu, A. R. Krauss, J. Luo, and X. Pan, Appl. Phys. Lett. **64(12)**, 1502 (1994).

[37]P. Kovarik, E. B. D. Bourdon, and R. H. Prince, Phys. Rev. B **48**, 12123 (1993).

[38]I. Jimenez, M. M. Garcia, J. M. Albella, and L. J. Terminello, Appl. Phys. Lett. **73**, 2911 (1998).

[39]S. Kunuku, K. J. Sankaran, C. L. Dong, N. H. Tai, K. C. Leou and I. N. Lin, RSC Adv. **4**, 47865 (2014).

Figure captions

FIG. 1. (a) Variation in the electrical conductivity (curve I, closed squares) and turn-on field (curve II, open circles) of nNCD films implanted with various dosages of Li-ions and subsequent annealing. (b) Field electron emission properties (current density-applied field, *J-E*, curves) measured in high vacuum environment for I. Li0. II. Li15 and III. Li15A films with the inset showing the corresponding Fowler-Nordheim (F-N) plots corresponding to the *J-E* curves. (c) The lifetime stability measurements (*J*-time curves) for Li15A films with the inset showing the lifetime stability measurements for Li15 films.

FIG. 2. SEM images of (a) Li15 films and (b) Li15A films; the inset in "a" shows the micro-Raman (λ=488.0 nm) spectra of I. Li15 and II. Li15A films; the inset in "b" shows the C1s XPS spectra of I. Li15 and II. Li15A films.

FIG. 3. (a) Bright-field TEM micrograph of Li15A films with corresponding SAED pattern shown as inset. (b) The high-resolution TEM micrograph of Li15A films corresponding to the regions "A" in "a". The inset FT_0 shows the Fourier-transformed image corresponding to the whole structure image. The ft_1 and ft_2 images show the FT images corresponding to regions "1" and "2" of the structure image, respectively.

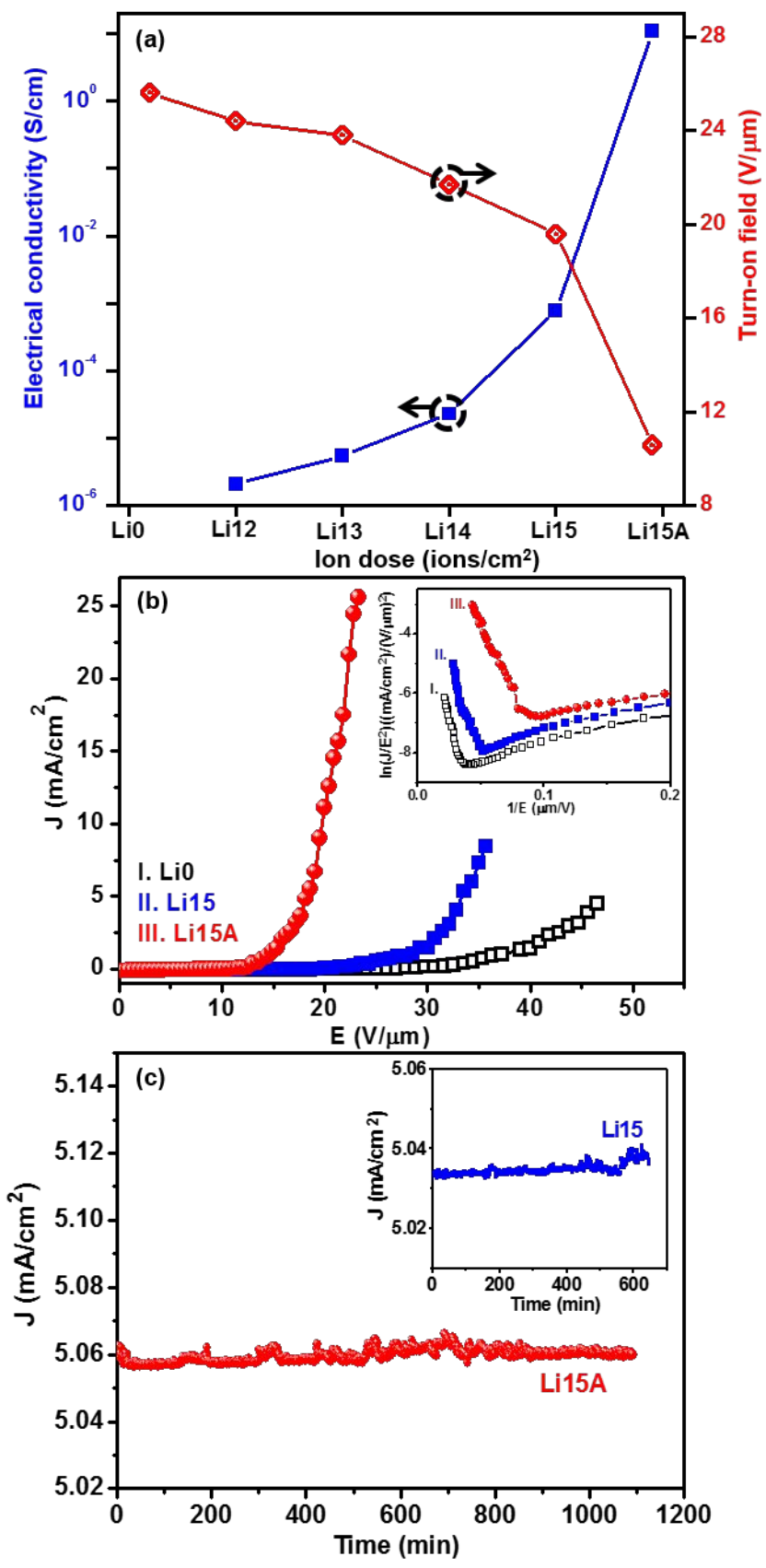
(a)
Electrical conductivity (S/cm)
Turn-on field (V/μm)
Li0
Li12
Li13
Li14
Li15
Li15A
Ion dose (ions/cm²)
(b)
J (mA/cm²)
I. Li0
II. Li15
III. Li15A
E (V/μm)
ln(J/E²)/((mA/cm²)/(V/μm)²)
1/E (μm/V)
(c)
J (mA/cm²)
Li15
Li15A
Time (min)

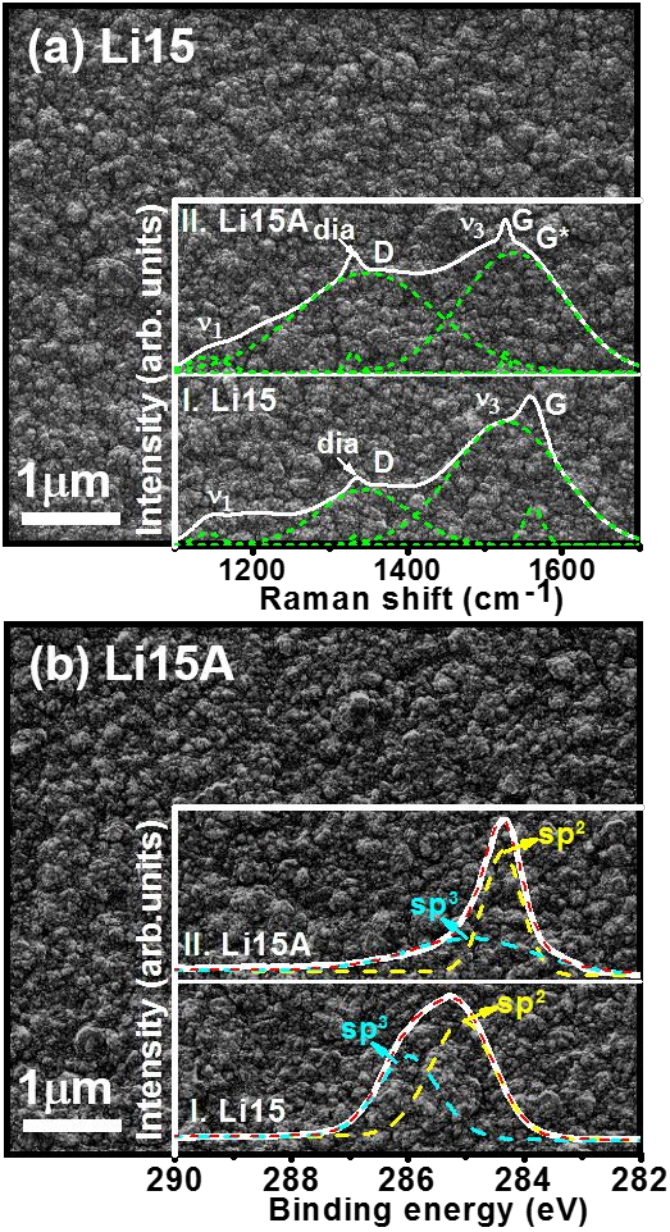
(a) Li15
II. Li15A
dia
D
ν_3
G
G*
ν_1
I. Li15
dia
D
ν_3
G
ν_1
Intensity (arb. units)
1μm
1200
1400
1600
Raman shift (cm^{-1})
(b) Li15A
II. Li15A
sp^2
sp^3
I. Li15
sp^2
sp^3
Intensity (arb.units)
1μm
290
288
286
284
282
Binding energy (eV)

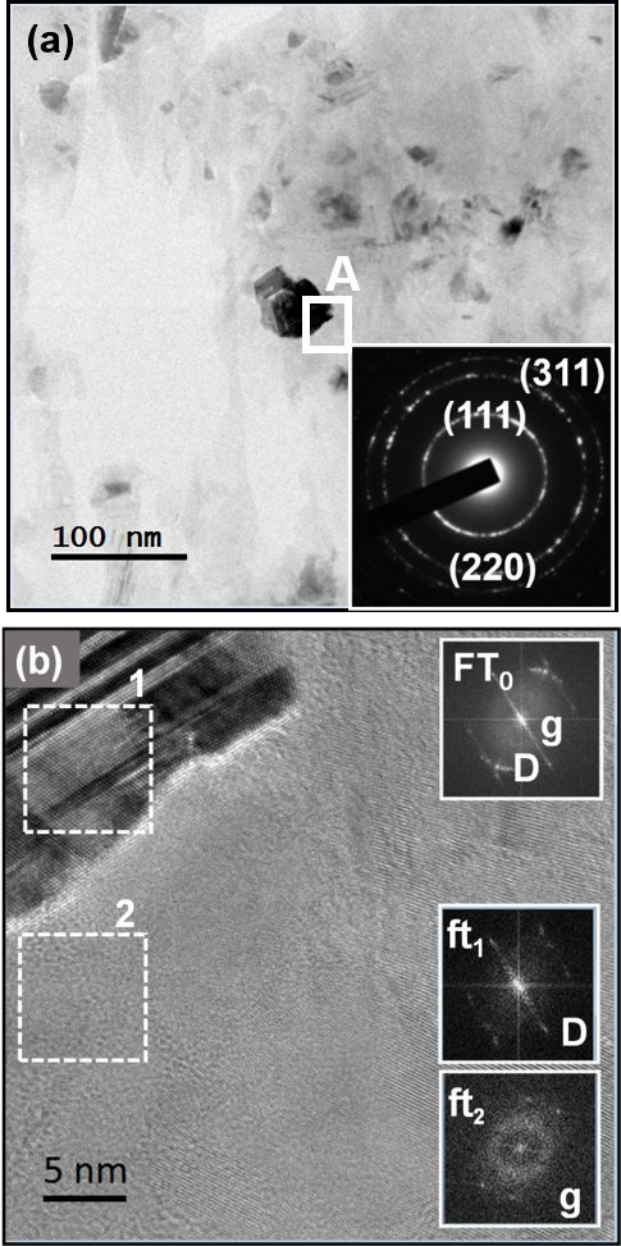
(a)
A
(311)
(111)
(220)
100 nm
(b)
1
2
FT0
g
D
ft1
D
ft2
g
5 nm